

Nucleon strange quark content from two-flavor lattice QCD with exact chiral symmetry

K. Takeda,¹ S. Aoki,^{1,2} S. Hashimoto,^{3,4} T. Kaneko,^{3,4} J. Noaki,³ and T. Onogi⁵

(JLQCD collaboration)

¹ *Graduate School of Pure and Applied Sciences,
University of Tsukuba, Tsukuba, Ibaraki 305-8571, Japan*

² *Center for Computational Sciences, University
of Tsukuba, Tsukuba, Ibaraki 305-8577, Japan*

³ *KEK Theory Center, High Energy Accelerator
Research Organization (KEK), Tsukuba 305-0801, Japan*

⁴ *School of High Energy Accelerator Science, The Graduate University
for Advanced Studies (Sokendai), Tsukuba 305-0801, Japan*

⁵ *Department of Physics, Osaka University, Toyonaka 560-0043, Japan*

(Dated: September 16, 2018)

Abstract

The strange quark content of the nucleon $\langle N|\bar{s}s|N\rangle$ is calculated in dynamical lattice QCD employing the overlap fermion formulation. For this quantity, exact chiral symmetry guaranteed by the Ginsparg-Wilson relation is crucial to avoid large contamination due to a possible operator mixing with $\bar{u}u + \bar{d}d$. Gauge configurations are generated with two dynamical flavors on a $16^3 \times 32$ lattice at a lattice spacing $a \simeq 0.12$ fm. We directly calculate the relevant three-point function on the lattice including a disconnected strange quark loop utilizing the techniques of the all-to-all quark propagator and low-mode averaging. Our result $f_{T_s} = m_s \langle N|\bar{s}s|N\rangle / M_N = 0.032(8)_{\text{stat}}(22)_{\text{sys}}$, where m_s and M_N are strange quark and nucleon masses, is in good agreement with our previous indirect estimate using the Feynman-Hellmann theorem.

I. INTRODUCTION

In the naive quark model, the nucleon consists of three valence up and down quarks. This picture is made more precise by taking account of quantum effects based on quantum chromodynamics (QCD), the fundamental theory of strong interaction, with which one expects additional effects due to the gluon and sea quark degrees of freedom. In fact, in high energy hadron scatterings, these effects are observed as parton distributions of the gluon and sea quarks, which can be analyzed using perturbative calculations of QCD. At low energy, quantitative calculation of the sea quark effect is far more difficult because of the nonperturbative nature of QCD. In this work, we consider the nucleon strange quark content $\langle N|\bar{s}s|N\rangle$. This matrix element directly measures the effect of sea quark, because there is no valence strange quark in the nucleon.

The nucleon strange quark content represents the effect of strange quark on the mass of the nucleon, which is often parametrized by

$$f_{T_s} = \frac{m_s \langle N|\bar{s}s|N\rangle}{M_N}, \quad (1)$$

where m_s and M_N are the masses of strange quark and nucleon. $\bar{s}s$ is the scalar operator made of strange quark fields. This parameter is also relevant to the dark matter searches, as one of the candidates —neutralino in the supersymmetric models— may interact with the nucleon most strongly through its strange quark content via the Higgs boson exchange diagram [1–5]. The magnitude of the matrix element $\langle N|\bar{s}s|N\rangle$ is therefore directly related to the sensitivity of the present [6, 7] and future experiments.

Another quantity of physical interest is a ratio of strange quark and light (up and down) quark contents:

$$y \equiv \frac{2 \langle N|\bar{s}s|N\rangle}{\langle N|\bar{u}u + \bar{d}d|N\rangle}. \quad (2)$$

The denominator $\langle N|\bar{u}u + \bar{d}d|N\rangle$ corresponds to the nucleon σ term, which is relatively well-determined as it is related to an amplitude of the pion-nucleon scattering. This is not the case for $\langle N|\bar{s}s|N\rangle$, for which only lattice QCD can potentially make a quantitative prediction.

The numerical calculation of the matrix element $\langle N|\bar{s}s|N\rangle$ on the lattice is not straightforward, because it involves a disconnected quark-loop diagram shown in Fig. 1. With the conventional method to calculate the quark propagator in lattice QCD, the computational

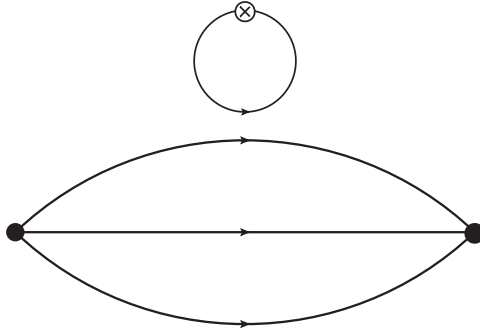


FIG. 1: Disconnected three-point function relevant to $\langle N|\bar{s}s|N\rangle$. Lines show quark propagators that are dressed by virtual gluons and sea quarks in QCD. The connected three lines correspond to the nucleon propagation and the disconnected loop arises from the strange scalar operator $\bar{s}s$.

cost to obtain the disconnected quark loop is prohibitively high, as one has to perform an expensive inversion of the Dirac operator for sources located at every lattice sites; the computational cost is then proportional to the lattice volume squared, $(N_s^3)^2$. Furthermore, since the scalar operator $\bar{s}s$ may have nonzero vacuum expectation value (VEV), which is divergent when m_s is finite, one has to subtract this VEV contribution to extract the physical matrix element $\langle N|\bar{s}s|N\rangle$. This requires a large cancellation that induces a large statistical error.

In this work, we overcome these practical difficulties in the lattice calculation by using the methods of the low-mode averaging [8, 9] and the all-to-all propagator [10, 11]. The all-to-all propagator allows us to calculate the propagation of the quark between arbitrary lattice sites at once, by introducing a stochastic estimator (for a practical implementation, see below). Although it introduces additional statistical noise, the low-mode averaging eliminates the noise for physically relevant low-lying quark-mode contributions and improves the statistics by averaging over space-time lattice sites. These techniques are crucial for the calculation of the disconnected diagram in lattice QCD.

Another important advantage of this work over the previous lattice calculations of $\langle N|\bar{s}s|N\rangle$ [12–15] is the use of a lattice fermion formulation that preserves exact chiral symmetry at finite lattice spacings. For both sea and valence quarks we employ the overlap fermion [16, 17], which satisfies the Ginsparg-Wilson relation [18] and thus has a symmetry under a modified chiral transformation [19]. This exact chiral symmetry prohibits the operator mixing under the renormalization between $\bar{s}s$ and $\bar{u}u + \bar{d}d$, where the matrix element of

the latter operator involves the connected diagram contribution. With the Wilson fermion formulation that has been used in the previous works, the operator mixing is induced due to the explicit chiral symmetry breaking on the lattice. Since the connected diagram contribution of $\bar{u}u + \bar{d}d$ is larger than the disconnected one by an order of magnitude, this may give rise to a large systematic error unless the mixing contribution is subtracted nonperturbatively.

In our previous work [20], we used a technique to extract $\langle N|\bar{u}u + \bar{d}d|N\rangle$ and $\langle N|\bar{s}s|N\rangle$ from the quark mass dependence of the nucleon mass using the Feynman-Hellman theorem. Since the number of sea quark mass values in the simulations was limited, the method had an inconsistency that the disconnected contribution was evaluated at up and down quark masses, which are different from the physical strange quark mass. In the present work, this limitation no longer remains. Although the calculation is done on two-flavor QCD lattices, which are available from the project of the dynamical overlap fermion by the JLQCD-TWQCD Collaboration [21], an extension to the realistic 2+1-flavor QCD is straightforward and in fact underway.

This paper is organized as follows. In Sec. II, our simulation setup and the methods of the all-to-all propagator and the low-mode averaging are described. We investigate the efficiency of the low-mode averaging by comparing the statistical error of the nucleon two-point function as presented in Sec. III. Extraction of the strange quark content from the disconnected three-point function is discussed in Sec. IV. Section V is devoted to a discussion of chiral extrapolation to the physical quark masses. In Sec. VI, we emphasize an important role of chiral symmetry in the calculation of the strange quark content. We also make a comparison with previous works including the recent results [22, 23]. Our conclusions are given in Sec. VII. A preliminary report of this work is found in [24].

II. SIMULATION DETAILS

A. Simulation Setup

On a four-dimensional Euclidean lattice we simulate QCD with two flavors of degenerate up and down quarks. As the lattice formulation, we use the Iwasaki gauge action and the

overlap quark action. The overlap-Dirac operator is given by [16, 17]

$$D(m) = \left(m_0 + \frac{m}{2}\right) + \left(m_0 - \frac{m}{2}\right) \gamma_5 \text{sgn}[H_W], \quad (3)$$

where $H_W = \gamma_5 D_W(-m_0)$ is the Hermitian Wilson-Dirac operator and $m_0 = 1.6$ in this study. The mass parameter m corresponds to the up-down or strange quark mass. We also introduce an additional Boltzmann factor [25] which does not change the continuum limit of the theory but substantially reduces the computational cost to calculate $\text{sgn}[H_W]$ by prohibiting the exact zero modes and suppressing near-zero modes of H_W . This additional Boltzmann factor induces a side effect that the *global* topological charge Q during the hybrid Monte Carlo update is fixed. We simulate only the trivial topological sector $Q = 0$ in this study; the effect of fixing topology is suppressed by an inverse power of the space-time volume $1/(N_s^3 N_t)$ [26] and turns out to be small (typically below a few percent level) in our studies of meson observables [27–29]. We expect that it is even smaller for baryons.

Our gauge configurations are generated on a $N_s^3 \times N_t = 16^3 \times 32$ lattice at a gauge coupling $\beta = 2.30$ where the lattice spacing is determined as $a = 0.118(2)$ fm using the Sommer scale $r_0 = 0.49$ fm as an input. We accumulate 100 independent configurations of two-flavor QCD at three values of up and down quark masses $m_{ud} = 0.025, 0.035, \text{ and } 0.050$, which cover a range of the pion mass $M_\pi = 370\text{--}520$ MeV. The physical quark masses are fixed as $m_{ud,\text{phys}} = 0.0034$ and $m_{s,\text{phys}} = 0.077$ from our analysis of the pion and kaon masses [28, 30]. We refer the readers to [21] for further details of the configuration generation.

We take two values of the valence strange quark mass $m_{s,\text{val}} = 0.070$ and 0.100 close to $m_{s,\text{phys}}$, and calculate two- and three-point functions

$$C_{2\text{pt}}^\Gamma(\mathbf{y}, t_{\text{src}}, \Delta t) = \frac{1}{N_s^3} \sum_{\mathbf{x}} \text{tr}_s [\Gamma \langle N(\mathbf{x}, t_{\text{src}} + \Delta t) \bar{N}(\mathbf{y}, t_{\text{src}}) \rangle], \quad (4)$$

$$C_{3\text{pt}}^\Gamma(\mathbf{y}, t_{\text{src}}, \Delta t, \Delta t_s) = \frac{1}{N_s^6} \sum_{\mathbf{x}, \mathbf{z}} \left\{ \text{tr}_s [\Gamma \langle N(\mathbf{x}, t_{\text{src}} + \Delta t) S^{\text{lat}}(\mathbf{z}, t_{\text{src}} + \Delta t_s) \bar{N}(\mathbf{y}, t_{\text{src}}) \rangle] \right. \\ \left. - \langle S^{\text{lat}}(\mathbf{z}, t_{\text{src}} + \Delta t_s) \rangle \text{tr}_s [\Gamma \langle N(\mathbf{x}, t_{\text{src}} + \Delta t) \bar{N}(\mathbf{y}, t_{\text{src}}) \rangle] \right\}, \quad (5)$$

where we use the nucleon interpolating field $N = \epsilon^{abc}(u_a^T C \gamma_5 d_b) u_c$ with the charge conjugation matrix $C = \gamma_4 \gamma_2$. The trace “ tr_s ” is over spinor index of the valence nucleon and $\langle \dots \rangle$ represents a Monte Carlo average. The scalar operator made of the strange quark field is given by

$$S^{\text{lat}} = \bar{s} \left(1 - \frac{D(0)}{2m_0} \right) s \quad (6)$$

on the lattice for the overlap-Dirac operator (3). To obtain the continuum operator $S^{\text{cont}}(\mu)$ at the energy scale μ , we need the renormalization factor $Z_S(\mu)$ as $S^{\text{cont}}(\mu) = Z_S(\mu)S^{\text{lat}}$. The details including possible operator mixing are discussed in Sec. VI.

We take two choices of the projection operator $\Gamma = \Gamma_{\pm} = (1 \pm \gamma_4)/2$, which correspond to the forward and backward propagating nucleons, respectively. The two- and three-point functions are averaged over the two choices of Γ

$$C_{2\text{pt}}(\mathbf{y}, t_{\text{src}}, \Delta t) = \frac{1}{2} \left\{ C_{2\text{pt}}^{\Gamma_+}(\mathbf{y}, t_{\text{src}}, \Delta t) + C_{2\text{pt}}^{\Gamma_-}(\mathbf{y}, t_{\text{src}}, N_t - \Delta t) \right\} \quad (7)$$

$$C_{3\text{pt}}(\mathbf{y}, t_{\text{src}}, \Delta t, \Delta t_s) = \frac{1}{2} \left\{ C_{3\text{pt}}^{\Gamma_+}(\mathbf{y}, t_{\text{src}}, \Delta t, \Delta t_s) + C_{3\text{pt}}^{\Gamma_-}(\mathbf{y}, t_{\text{src}}, N_t - \Delta t, N_t - \Delta t_s) \right\} \quad (8)$$

in order to reduce statistical errors.

B. All-to-all quark propagator

The three-point correlation function $C_{3\text{pt}}$ is calculated by appropriately connecting the quark propagator $D^{-1}(x, y)$ as shown in Fig. 1. The conventional method to calculate the quark propagator is not suitable to construct the disconnected quark loop starting from and ending at arbitrary lattice sites since the source point y has to be fixed at a certain lattice site. Indeed, we use the all-to-all quark propagator technique, which enables propagations from any lattice site to any site, following the strategy proposed in [10, 11].

It is expected that low-lying eigenmodes of $D(m)$ dominantly contribute to the low-energy dynamics of QCD. We calculate the low-lying eigenvalues and eigenvectors using the implicitly restarted Lanczos algorithm, from which we can construct their contribution to the quark propagator *exactly* as

$$(D^{-1}(m))_{\text{low}}(x, y) = \sum_{i=1}^{N_e} \frac{1}{\lambda^{(i)}(m)} v^{(i)}(x) v^{(i)}(y)^\dagger, \quad (9)$$

where $\lambda^{(i)}(m)$ and $v^{(i)}(x)$ represent the i -th lowest eigenvalue and its associated eigenvector of $D(m)$, respectively. Note that the eigenvectors are independent of valence quark masses. The number of low-lying eigenmodes N_e we calculated is 100 in this study.

The remaining high-mode contribution is estimated stochastically. We prepare a single Z_2 noise vector $\eta(x)$ for each configuration and split it into $N_d = 3 \times 4 \times N_t/2$ vectors $\eta^{(d)}(x)$ ($d = 1, \dots, N_d$), which have nonzero elements only for a single combination of color and

spinor indices on two consecutive time slices. The high-mode contribution is then estimated as

$$(D^{-1}(m))_{\text{high}}(x, y) = \sum_{d=1}^{N_d} \psi^{(d)}(x) \eta^{(d)}(y)^\dagger, \quad (10)$$

where $\psi^{(d)}(x)$ is obtained by solving a linear equation for each noise vector

$$D(m)\psi^{(d)}(x) = (1 - \mathcal{P}_{\text{low}})\eta^{(d)}(x) \quad (d = 1, \dots, N_d). \quad (11)$$

\mathcal{P}_{low} is a projector to the subspace spanned by the low-modes

$$\mathcal{P}_{\text{low}}(x, y) = \sum_{i=1}^{N_e} v^{(i)}(x) v^{(i)}(y)^\dagger. \quad (12)$$

We use this all-to-all propagator, namely, (9) plus (10), to calculate the disconnected quark loop and the vacuum expectation value of S^{lat} in $C_{3\text{pt}}$.

C. Low-mode averaging

In principle, we can use the all-to-all propagator to calculate nucleon correlators, namely, $C_{2\text{pt}}$ and the piece representing the nucleon propagation in $C_{3\text{pt}}$. However, these quantities decay exponentially as the temporal separation Δt increases, so that the contributions to the nucleon correlator from the high-modes (10) are not sufficiently precise at large Δt when we take only one noise sample for each configuration.

In this study, we therefore use the low-mode averaging (LMA) technique proposed in [8, 9]. Suppose that we decompose the conventional quark propagator into its low-mode part, which is in the subspace spanned by the low-modes and the remaining high-mode part. We can then write $C_{2\text{pt}}$ in terms of the following eight contributions:

$$C_{2\text{pt}} = C_{2\text{pt}}^{\text{lll}} + C_{2\text{pt}}^{\text{llh}} + C_{2\text{pt}}^{\text{hlh}} + C_{2\text{pt}}^{\text{hll}} + C_{2\text{pt}}^{\text{dlh}} + C_{2\text{pt}}^{\text{hhl}} + C_{2\text{pt}}^{\text{hhl}} + C_{2\text{pt}}^{\text{hhh}}. \quad (13)$$

Here, $C_{2\text{pt}}^{\text{lll}}$ is constructed only by the low-mode part of the quark propagator; $C_{2\text{pt}}^{\text{llh}}$ is the one in which two of the valence quarks are made of low-modes and the other is the high-mode part. The other combinations are understood in a similar manner. Since the ensemble average can be taken for each term of (13), we attempt to reduce the statistical error for individual contributions.

Relying on the translational invariance, we may replace $C_{2\text{pt}}^{\text{lll}}$ by a more precise estimate by averaging over the location of the nucleon source point $(\mathbf{y}, t_{\text{src}})$. No additional inversion of

the Dirac operator is necessary to take the average, as we can explicitly use the representation (9) made of low-mode eigenvectors. This LMA technique is very effective in reducing the statistical error of $C_{2\text{pt}}$ at large Δt when $C_{2\text{pt}}$ is well dominated by $C_{2\text{pt}}^{ll}$.

In this study, we employ LMA to calculate $C_{2\text{pt}}$ and the nucleon piece of $C_{3\text{pt}}$. We also test an extension in which additional three contributions, $C_{2\text{pt}}^{llh}$, $C_{2\text{pt}}^{hlh}$, and $C_{2\text{pt}}^{hll}$, are averaged over the source location by using the all-to-all propagator. The signal may be improved if the reduction of the statistical error by the source average outweighs the induced noise from the high-modes. The result of the test is shown in the next section.

D. Smeared nucleon operators

Since $C_{2\text{pt}}$ and $C_{3\text{pt}}$ decay quickly as a function of Δt , we need to use smeared nucleon operator that suppresses excited-state contaminations at small Δt .

For the (local or smeared) quark field, we consider the following three choices:

1. local

$$q_{\text{loc}}(\mathbf{x}, t) = q(\mathbf{x}, t). \quad (14)$$

2. exponential smearing

$$q_{\text{smr}}^{\text{exp}}(\mathbf{x}, t) = \sum_{\mathbf{r}} \exp(-B|\mathbf{r}|) q(\mathbf{x} + \mathbf{r}, t), \quad (15)$$

where the parameter B is set to 0.350, 0.375, 0.400 at $m_{ud} = 0.025, 0.035, 0.050$, respectively.

3. Gaussian smearing

$$q_{\text{smr}}^{\text{gss}}(\mathbf{x}, t) = \sum_{\mathbf{y}} \left\{ \left(\mathbb{1} + \frac{\omega}{4N} H \right)^N \right\}_{\mathbf{x}, \mathbf{y}} q(\mathbf{y}, t), \quad H_{\mathbf{x}, \mathbf{y}} = \sum_{i=1}^3 (\delta_{\mathbf{x}, \mathbf{y} - \hat{i}} + \delta_{\mathbf{x}, \mathbf{y} + \hat{i}}), \quad (16)$$

where the parameters $\omega = 20$ and $N = 400$ are chosen so that the extent of the smeared operator is roughly equal to that of (15) with $B = 0.400$.

Then, the nucleon interpolating fields $N_{\text{loc}}(\mathbf{x}, t)$, $N_{\text{smr}}^{\text{exp}}(\mathbf{x}, t)$, $N_{\text{smr}}^{\text{gss}}(\mathbf{x}, t)$, are constructed from the corresponding local or smeared quark fields.

When we smear the quark field, we fix the gauge to the Coulomb gauge. With this choice one can avoid significant statistical noise coming from the fluctuation of the gauge link.

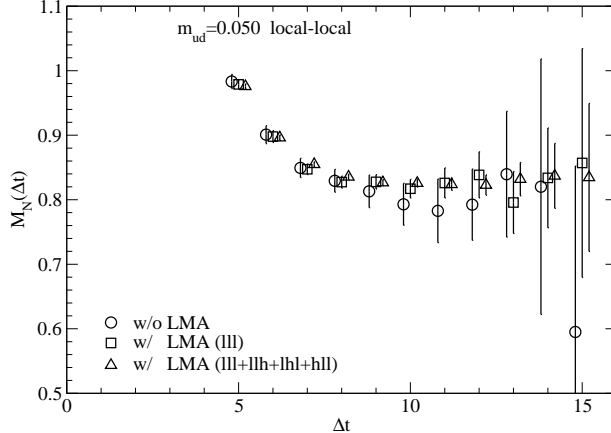


FIG. 2: Effective mass $M_N(\Delta t)$ from the nucleon two-point function $C_{2\text{pt}}$ at $m_{ud} = 0.050$. The local operator is used for both source and sink. Circles show the result of the conventional point source, while squares (triangles) are obtained by averaging the $C_{2\text{pt}}^{lll}$ ($C_{2\text{pt}}^{lll} + C_{2\text{pt}}^{llh} + C_{2\text{pt}}^{hlh} + C_{2\text{pt}}^{hll}$) contributions. Circles and triangles are slightly shifted in the horizontal direction for clarity.

The Gaussian smearing is particularly useful for the sink smearing, since the number of numerical operation $\sim N \times N_s^3$ is smaller than $\sim N_s^6$ for the case of (15).

III. IMPROVING THE NUCLEON TWO-POINT FUNCTION

Since the disconnected three-point function $C_{3\text{pt}}$ is extremely noisy, it is crucial to reduce the statistical noise and to extract the signal at relatively small time separations. We therefore tested various methods to improve the signal on the nucleon two-point functions $C_{2\text{pt}}$ before applying them to the three-point functions.

A. Low-mode averaging

As mentioned in the previous section, we consider two options: (i) to average only $C_{2\text{pt}}^{lll}$ over the source locations, (ii) to average also $C_{2\text{pt}}^{llh} + C_{2\text{pt}}^{hlh} + C_{2\text{pt}}^{hll}$. The second choice requires the high-mode of the quark propagator $(D^{-1})_{\text{high}}(x, y)$, which is calculated stochastically as in (10).

In Fig. 2 we plot the nucleon effective mass $M_N(\Delta t)$ with the local source and sink operators at our heaviest quark mass $m_{ud} = 0.050$. The data without LMA (circles) show a rapidly growing statistical error as Δt increases, so that the error at $\Delta t = 10$ where

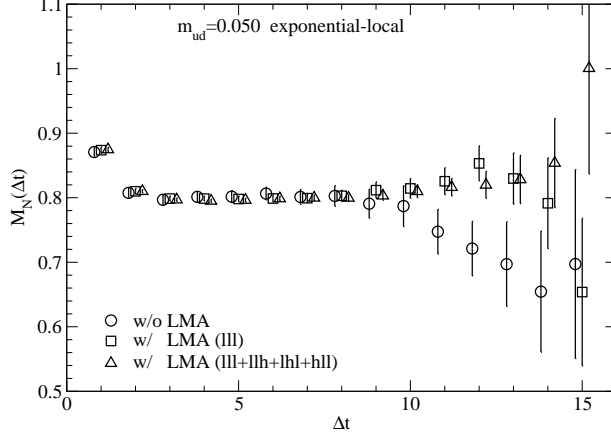


FIG. 3: Effective mass $M_N(\Delta t)$ from $C_{2\text{pt}}$ with an exponentially smeared source at $m_{ud} = 0.050$. The symbols are the same as in Fig. 2.

the plateau is approximately reached is already as large as 4%. By averaging over the source locations for $C_{2\text{pt}}^{lll}$ (squares), the statistical error is reduced by a factor of about 3. Further improvement of a factor of 2 is possible if we average over the source points also for $C_{2\text{pt}}^{llh} + C_{2\text{pt}}^{lhl} + C_{2\text{pt}}^{hll}$, as shown by triangles.

A similar comparison of $M_N(\Delta t)$ at $m_{ud} = 0.050$ but with the exponentially smeared source and a local sink is shown in Fig. 3. (But LMA is done over a limited number of the source location $N_{\text{src}} = N_t \times 16$. For discussions, see below.) We observe that LMA for $C_{2\text{pt}}^{lll}$ is efficient when combined with the smeared source, while the effect of the extended LMA for $C_{2\text{pt}}^{llh} + C_{2\text{pt}}^{lhl} + C_{2\text{pt}}^{hll}$ is not substantial, i.e., the reduction of statistical error is only about 30%.

Although the effect of LMA to reduce the statistical noise is significant, it is also true that it requires substantial computational effort. If we average over the entire space-time source points, the computational cost scales as $(N_s^3 \times N_t)^2$, which is prohibitive unless we use the fast Fourier transform. If we combine LMA with the smeared source, another factor of N_s^3 is necessary, which is not feasible any more. We therefore consider averaging over a limited number of source locations. Since the correlators from different source points are statistically highly correlated, this might not spoil the efficiency of LMA largely.

In Fig. 4, we compare the data of $M_N(\Delta t)$ obtained using LMA with a different number of source points averaged N_{src} . The plot shows the results of LMA for both $C_{2\text{pt}}^{lll}$ and $C_{22\text{pt}}^{llh} + C_{2\text{pt}}^{lhl} + C_{2\text{pt}}^{hll}$ with $N_{\text{src}} = N_t$ (squares), $N_t \times 8$ (triangles down), and $N_t \times 16$ (triangles up).

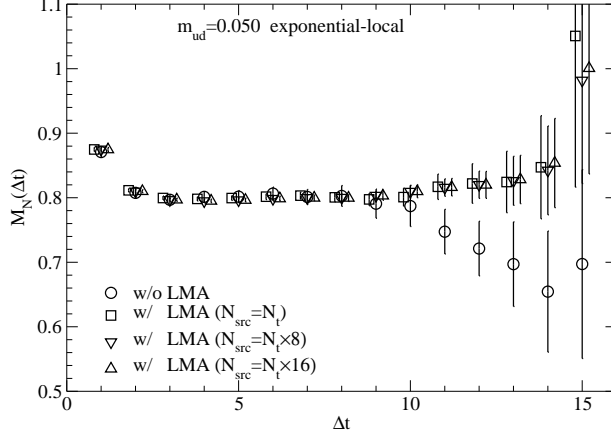


FIG. 4: Comparison of $M_N(\Delta t)$ obtained with different numbers of source locations for LMA. Circles are those without LMA. Results averaged over the time slices are shown by squares. We obtain down- and up-triangles by further averaging over 8 and 16 spatial sites at each time slice, respectively. In the plot, N_{src} represents the number of the source locations.

For $N_{\text{src}} = N_t$, the spatial location of the source is fixed and the average is taken over N_t time slices. For $N_{\text{src}} = N_t \times 8$, points of spatial coordinates 0 or $N_s/2$ in three spatial dimensions are all averaged; for $N_t \times 16$, we also average over $(N_s/4, N_s/4, N_s/4)$, $(N_s/4, N_s/4, 3N_s/4)$, $(N_s/4, 3N_s/4, 3N_s/4)$, and $(3N_s/4, 3N_s/4, 3N_s/4)$ (and all possible permutations) for each time slice.

From Fig. 4 we observe that the result with $N_{\text{src}} = N_t$ is already very good, while the improvement with $N_{\text{src}} = N_t \times 8$ is not substantial. Beyond this number, we do not gain significant improvement. Note that the maximal number of points we took $N_{\text{src}} = N_t \times 16$ corresponds to the data shown in Fig. 3 (triangles).

Overall, taking the cost of numerical calculation into account, the best choice would be $N_{\text{src}} \sim N_t \times 8$; in our following analysis we choose $N_{\text{src}} \sim N_t \times 16$, which has been still doable. The advantage of LMA for $C_{2\text{pt}}^{lll}$ is always clear, while that for $C_{2\text{pt}}^{llh} + C_{2\text{pt}}^{hlh} + C_{2\text{pt}}^{hll}$ depends on the channel or source operator. Therefore, we average only $C_{2\text{pt}}^{lll}$ when we use the smeared sink, which is numerically more costly.

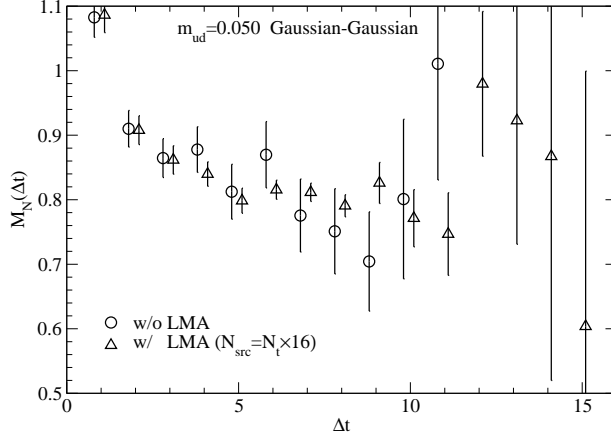


FIG. 5: Effective mass $M_N(\Delta t)$ with the Gaussian smeared source and sink at $m_{ud} = 0.050$. Circle are without LMA; triangles are obtained by averaging C_{2pt}^{lll} over 16 spatial sites at each time slice.

B. Sink smearing

The smearing of the source operator is routinely used in many lattice calculations. It is designed to deplete the overlap with excited-state contributions so that the plateau of the effective mass constructed from the two-point correlator appears earlier in Δt . By using the smeared operator also for the sink we expect that the excited-state contaminations are further reduced, but usually the benefit is not clearly seen mainly because the statistical noise increases with the smeared sink. Since the numerical cost for the sink smearing is high in general [$\sim (N_s^3)^2$], it has not been commonly used.

The situation may be different for three-point functions, where an operator is inserted in the middle of the two-point function. Here the nucleon and its excited states are created at the smeared source point and propagate until the point of the operator is reached. Between these two points, the depletion of the excited states is at work because of the smeared source. After the insertion of the operator, the nucleon and its excited states propagate until they are absorbed by the sink. In this second propagation, the excited states are not necessarily suppressed, since the operator insertion may excite the nucleon, i.e., $\langle N | \bar{s}s | N' \rangle \neq 0$, and the sink operator may have substantial overlap with the excited state $|N'\rangle$. This is indeed the case in our calculation of the three-point function relevant to the strange quark content, as we will see in the next section.

We therefore utilize the smeared operator also for the sink. Since the conventional choice

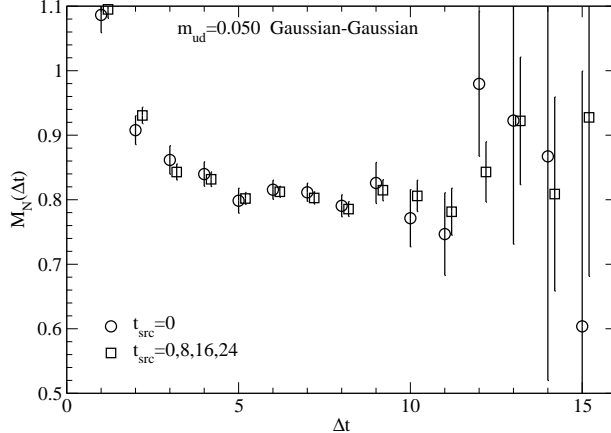


FIG. 6: Improving the statistics by averaging the nucleon two-point functions calculated from four different source points at time slices $t_{src} = 0, 8, 16,$ and 24 . The result for $M_N(\Delta t)$ (squares) is compared with that without the average, i.e., $t_{src} = 0$. The quark mass is $m_{ud} = 0.050$. The Gaussian smearing is used for both the nucleon source and sink.

$q_{smr}^{\text{exp}}(\mathbf{x}, t)$ (15) requires a numerical cost proportional to N_s^3 for each (\mathbf{x}, t) , we use $q_{smr}^{\text{gss}}(\mathbf{x}, t)$ (16), instead. Figure 5 shows $M_N(\Delta t)$ with this Gaussian smeared operator for both the source and sink. Although the statistical signal is worse compared to the case of the local sink shown in Fig. 3 and 4, we may improve it using LMA for C_{2pt}^{lll} as shown in Fig. 5 by triangles. Further improvement is not expected with the average over $C_{2pt}^{llh} + C_{2pt}^{lhl} + C_{2pt}^{hll}$, as in the case of the smeared source and local sink (Fig. 3).

C. Duplication

Instead, we simply repeat the calculation 4 times by setting the source at different time slices. Namely, we calculate the nucleon two-point function locating the source on the time slices $t_{src} = 8, 16,$ and 24 , in addition to the original choice $t_{src} = 0$, and average over these duplicated correlators. The effect is shown in Fig. 6, where we observe a reduction of the statistical error by a factor of 2 at large time separations. However, we find that the further average of the duplicated correlators is not substantial. This is tested at $m_{ud} = 0.025$ by calculating the nucleon two-point function locating the source on the time slices $t_{src} = 4, 12, 20,$ and 28 besides $t_{src} = 0, 8, 16, 24$. Therefore, we restrict the number of the duplication of the nucleon two-point function for other quark masses.

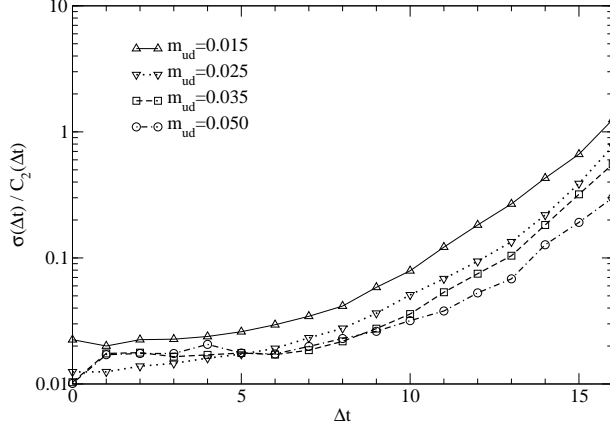


FIG. 7: Noise-to-signal ratio of the nucleon correlator at $m_{ud} = 0.015, 0.025, 0.035,$ and 0.050 .

Source-sink	N_{src}	LMAed contribution	Duplication
Local-local	$N_t \times N_s$	$C_{2\text{pt}}^{lll} + C_{2\text{pt}}^{llh} + C_{2\text{pt}}^{lhl} + C_{2\text{pt}}^{hll}$	1
Exponential-local	$N_t \times 16$	$C_{2\text{pt}}^{lll} + C_{2\text{pt}}^{llh} + C_{2\text{pt}}^{lhl} + C_{2\text{pt}}^{hll}$	1
Gaussian-Gaussian	$N_t \times 16$	$C_{2\text{pt}}^{lll}$	4 or 8

TABLE I: Choices of the scheme of averaging the nucleon correlator in this work. For different smearing operators at the source and sink, we list the number of source points N_{src} averaged in LMA, the contributions to the correlator averaged in LMA ($C_{2\text{pt}}^{lll}$ or $C_{2\text{pt}}^{lll} + C_{2\text{pt}}^{llh} + C_{2\text{pt}}^{lhl} + C_{2\text{pt}}^{hll}$), and the number of the duplications of the conventional correlators.

Figure 7 shows the increase of the statistical noise in $C_{2\text{pt}}$ for the case of smeared source and sink. The plot shows the data at four different quark masses $m_{ud} = 0.015, 0.025, 0.035,$ and 0.050 . As expected, the noise grows more rapidly for lighter quarks. Since the plateau in the effective mass is reached at around $\Delta t = 5$, we need at least $\Delta t = 10$ in the calculation of the three-point functions. At the lightest quark mass $m_{ud} = 0.015$, the error around $\Delta t = 10$ is too large ($\sim 10\%$) to be useful in the analysis of the disconnected three-point functions. We therefore discard this data point in the analysis of the strange quark content.

In order to optimize the statistical signal in the calculation of the disconnected three-point function for a given amount of computer time, we choose different schemes of averaging the correlators depending on the source and sink smearing combinations. These include the choices of the contributions averaged in LMA ($C_{2\text{pt}}^{lll}$ or $C_{2\text{pt}}^{lll} + C_{2\text{pt}}^{llh} + C_{2\text{pt}}^{lhl} + C_{2\text{pt}}^{hll}$), the number

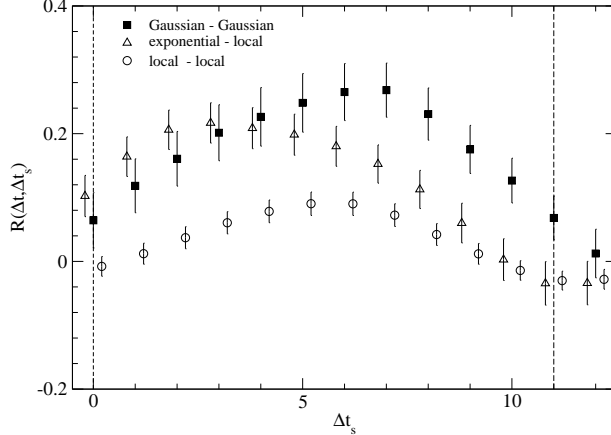


FIG. 8: Ratio $R(\Delta t, \Delta t_s)$ with $\Delta t = 11$ at $m_{ud} = 0.050$ and $m_{s, val} = 0.100$. Circles (triangles) are results obtained with the local (exponentially smeared) source and local sink, whereas squares are calculated using the Gaussian smeared source and sink. The vertical lines show the locations of the nucleon operators. The noisy high-mode contribution to the quark loop is ignored in this plot.

of source points N_{src} averaged in LMA, as well as the number of the duplications of the conventional correlators. Our choices in this work are listed in Table I.

IV. EXTRACTION OF THE STRANGE QUARK CONTENT

A. Finding a plateau in the three-point function

We extract the strange quark content on the lattice $\langle N|S^{\text{lat}}|N \rangle$ from a ratio of $C_{3\text{pt}}(\Delta t, \Delta t_s)$ and $C_{2\text{pt}}(\Delta t)$

$$R(\Delta t, \Delta t_s) \equiv \frac{C_{3\text{pt}}(\Delta t, \Delta t_s)}{C_{2\text{pt}}(\Delta t)} \xrightarrow{\Delta t, \Delta t_s \rightarrow \infty} \langle N|S^{\text{lat}}|N \rangle \quad (17)$$

where Δt is the temporal interval between the nucleon source and sink. The scalar operator S^{lat} is set on the time slice apart from the nucleon source by Δt_s . Note that $C_{3\text{pt}}(\Delta t, \Delta t_s)$ and $C_{2\text{pt}}(\Delta t)$ are calculated with LMA. We suppress the coordinates of the nucleon source location $(\mathbf{y}, t_{\text{src}})$ presented in (7) and (8).

In order to extract $\langle N|S^{\text{lat}}|N \rangle$, we first have to identify a plateau in the ratio $R(\Delta t, \Delta t_s)$ at sufficiently large Δt and Δt_s . For this purpose, we look at the same ratio but approximated by taking only the low-mode contribution in the strange quark loop. Namely, the piece

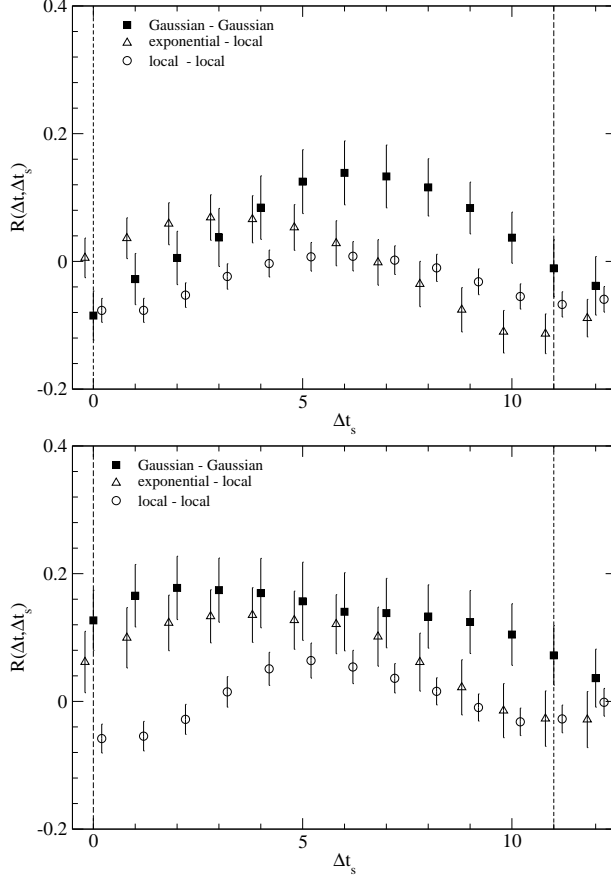


FIG. 9: Same as Fig. 8, but for $m_{ud} = 0.035$ (top panel) and $m_{ud} = 0.025$ (bottom panel).

of $S^{\text{lat}}(z)$ in (5) is replaced by its low-mode contribution $\text{Tr}[(D^{-1}(m))_{\text{low}}(z, z)]$. We expect that the ratio $R(\Delta t, \Delta t_s)$ is dominated by this low-mode contribution, because the high-mode contribution that leads to the ultraviolet divergence in the continuum limit cancels by the VEV subtraction in (5). Low-energy physics must be well described by the low-mode contribution in the strange quark loop. This approximation is finally removed in our calculation by the full calculation, but here we consider the approximately calculated ratio to identify the plateau, where the ground-state nucleon dominates.

Figure 8 shows the approximated ratio obtained at $m_{ud} = 0.050$ and $m_{s, \text{val}} = 0.100$ with various combinations of the source and sink smearing. The separation between the source and sink is fixed to $\Delta t = 11$, and the location of the scalar operator Δt_s is varied. Thus, we expect a signal around $\Delta t_s \sim \Delta t/2$. We observe a plateau between $\Delta t_s = 3$ and 8, when the source and sink operators are both smeared with the Gaussian smearing (16), as shown by filled squares. The data with the local source and sink (open circles) show a slight increase

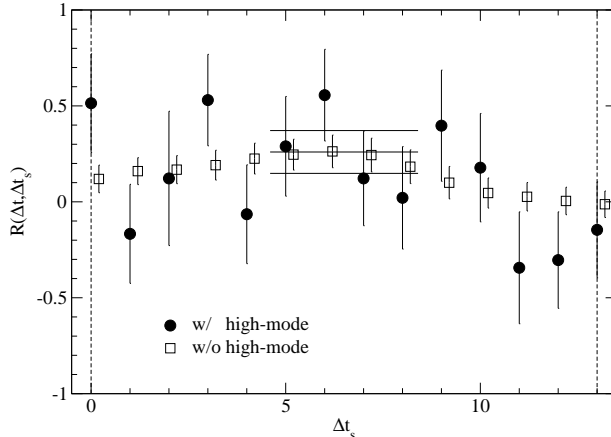


FIG. 10: Ratio $R(\Delta t = 13, \Delta t_s)$ at $m_{ud} = 0.050$ and $m_{s, val} = 0.100$ with (filled circles) and without the high-mode contribution to the strange quark loop (open squares). The horizontal lines show the result of a constant fit $R(\Delta t)$ and its error band.

in the same region but do not reach the value of the plateau for the smeared source-sink combination.

The data of the smeared source and local sink (open triangles) show a bump around $\Delta t_s \sim 2 - 6$ and decrease towards $\Delta t_s = 11$, so that the plot looks asymmetric. This can be explained by an excited-state contamination on the sink side ($\Delta t_s = 11$) because the sink operator is local. Therefore, unlike the case for the two-point function, the use of the smeared operator for both source and sink is essential for the three-point function in order to extract the ground-state signal.

Similar plots are shown for $m_{ud} = 0.035$ and 0.025 in Fig. 9. We observe similar behavior of the approximated ratio.

B. Bare results for the strange quark content

The ratio $R(\Delta t, \Delta t_s)$ in (17) without the low-mode approximation is shown in Fig. 10 (filled circles) together with that of the low-mode approximation (open squares). Here, the data for $\Delta t = 13$ are shown. Although the statistical noise is much larger when the high-mode contributions are included, the central value is unchanged.

Since the high-mode contributions are calculated with random noise (10), the larger noise is expected. But, because the noise given for each time slice is statistically independent, the

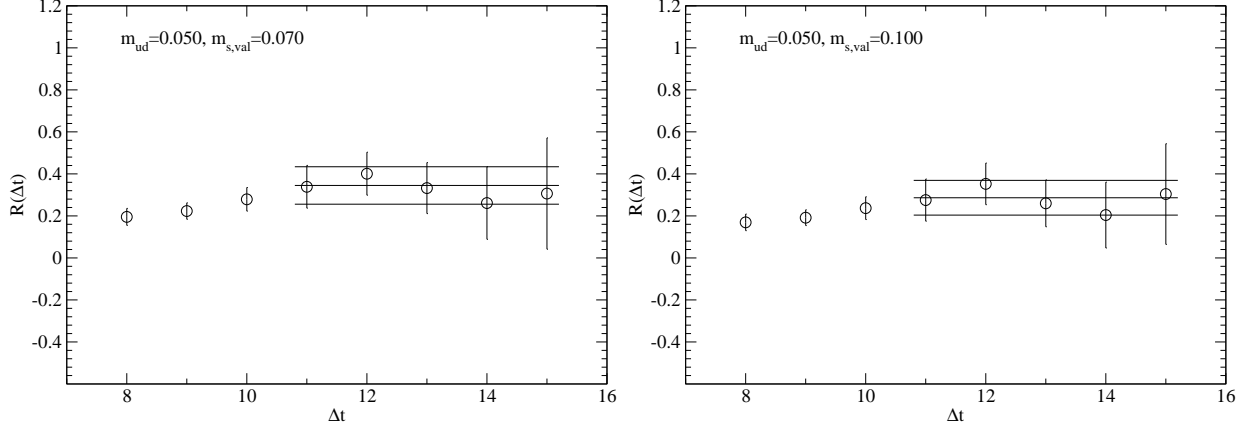


FIG. 11: Results of the constant fit for $R(\Delta t, \Delta t_s)$ in the range $\Delta t_s = [5, \Delta t - 5]$. The data at $m_{ud} = 0.050$. The left and right panels show those at $m_{s,val} = 0.070$ and 0.100 , respectively.

correlation among the data points at different Δt_s is expected to come mainly from the low modes, provided that the high-mode contribution to the ratio is negligible, which is indeed the case within our statistical accuracy. The statistical error is then effectively reduced by averaging over different Δt_s . In Fig. 10, the result of a constant fit for $\Delta t_s = [5, 8]$ is shown by a horizontal line together with a band showing the resulting statistical error. In this case, the statistical error of the fitted value is about a half of that of each point, because four data points are averaged. We also checked that the statistical correlation among the points at different Δt_s is an order of magnitude smaller than the variance of each point.

For the final result, we take the full data including the high modes and fit in the region where the approximated ratio shows a plateau. To be specific, we fit in the region $\Delta t_s = [5, \Delta t - 5]$ with $\Delta t \geq 11$.

Figures 11–13 show the results of the constant fit for each Δt . We find that the results are stable under the change of Δt . We then fit these results by a constant in $\Delta t = [11, 15]$. The statistical error is estimated using the jackknife method. The numerical results are listed in Table II.

In order to estimate the systematic effect due to possible contamination of the excited states, we also test a fitting form for $R(\Delta t, \Delta t_s)$ taking account of the first excited state:

$$R(\Delta t, \Delta t_s) = c_0 - c_1 e^{-(2M_0 + \Delta M)\Delta t/2} \cosh(\Delta M(\Delta t_s - \Delta t/2)), \quad (18)$$

where the first and second terms represent the contributions from the ground and first excited states, respectively. ΔM is the mass gap between these two states. To make this

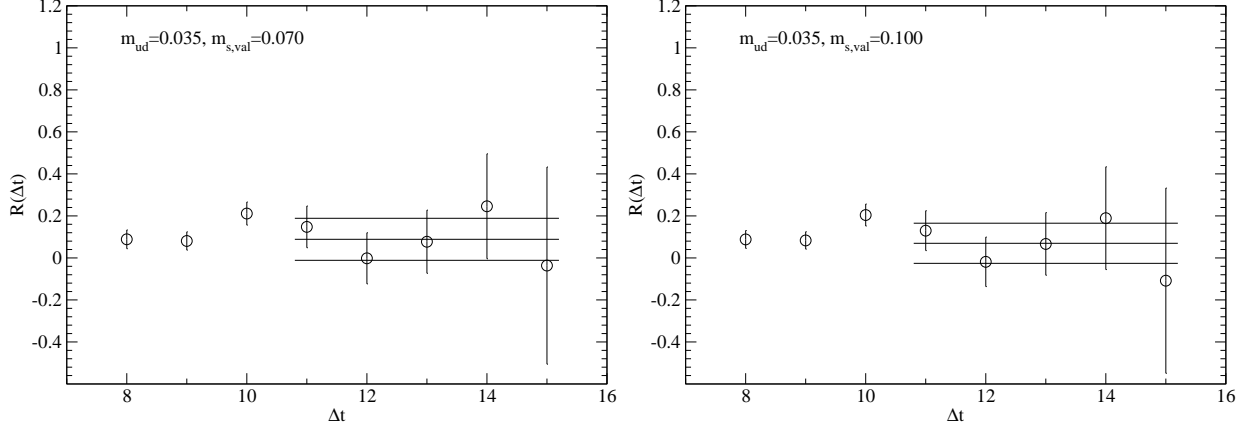


FIG. 12: Same as Fig. 11 but at $m_{ud} = 0.035$.

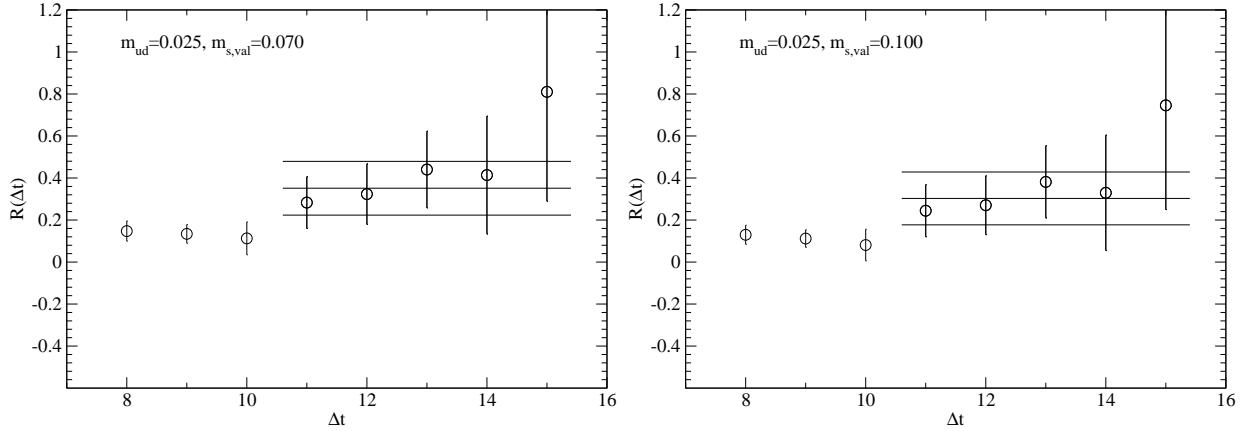


FIG. 13: Same as Fig. 11 but at $m_{ud} = 0.025$.

fit stable, we carry out a simultaneous fit in terms of Δt_s and Δt using a slightly wider fit range, $\Delta t_s = [4, \Delta t - 4]$ and $\Delta t \geq 11$. We also use the ground-state mass M_0 determined from the nucleon two-point function. The excited-state contribution represented by the c_1 term turned out to be small: in the maximum case ($\Delta t = 11$) it is about $0.04(8)$ compared to the main contribution $c_0 \simeq 0.3(1)$. For large Δt , the excited-state contribution is more suppressed. This is expected from the small Δt_s and Δt dependence of the ratio shown in Figs.10–13. We therefore use the results in Table II in the following analysis without adding further errors due to the excited states.

m_{ud}	Fit range of Δt	$m_{s,val} = 0.070$	$m_{s,val} = 0.100$
0.050	[11,15]	0.345(89)	0.286(83)
0.035	[11,15]	0.089(100)	0.070(96)
0.025	[11,15]	0.351(128)	0.303(126)

TABLE II: Strange quark content $\langle N|S^{\text{lat}}|N\rangle$ calculated on the lattice at each quark mass. The fit range of Δt is also listed.

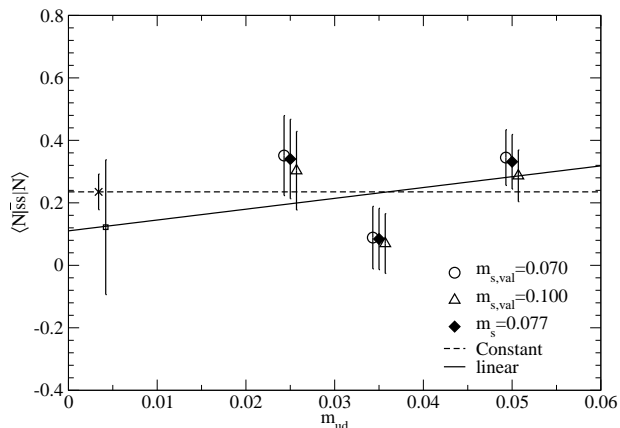


FIG. 14: The dependence of $\langle N|S^{\text{lat}}|N\rangle$ on the up and down quark mass m_{ud} (given in the lattice unit). Open circles and triangles are the data at each m_{ud} and $m_s = 0.070$ (circles) and 0.100 (triangles). The data linearly interpolated to the physical strange quark mass $m_{s,\text{phys}}$ is shown by filled diamonds. Dashed and solid lines show the fit curve at $m_{s,\text{phys}}$ obtained from the constant and linear extrapolations.

V. CHIRAL EXTRAPOLATION TO THE PHYSICAL POINT

In this section, we discuss on the extrapolation of our lattice data to the physical quark masses. We have three data points corresponding to up and down quark masses m_{ud} in the range of $M_\pi = 370\text{--}520$ MeV. For the strange quark mass we have two data points sandwiching the physical strange quark mass.

Our data for the matrix element $\langle N|S^{\text{lat}}|N\rangle$ are plotted as a function of m_{ud} in Fig. 14. We do not observe statistically significant dependence of $\langle N|S^{\text{lat}}|N\rangle$ on both m_{ud} and m_s .

	$\chi^2/\text{d.o.f.}$	d.o.f.	c_0	$c_{1,ud}$	$c_{1,s}$	$\langle N S^{\text{lat}} N\rangle$
constant	1.63	5	0.24(6)	0.24(6)
linear	2.39	3	0.22(24)	3.5(5.7)	-1.44(52)	0.12(22)

TABLE III: Numerical results of chiral extrapolation. We also list $\langle N|S^{\text{lat}}|N\rangle$ extrapolated to the physical point.

By fitting the data linearly in m_{ud} and m_s as

$$\langle N|S^{\text{lat}}|N\rangle = c_0 + c_{1,ud}m_{ud} + c_{1,s}m_{s, \text{val}}, \quad (19)$$

we obtain the numerical results of the fit parameters c_0 , $c_{1,ud}$, and $c_{1,s}$ listed in Table III. We also show the result of a constant fit including only the c_0 term in (19). Both results are consistent with each other, but the linear extrapolation gives a larger error at the physical point.

Assuming that the quark mass dependence of the nucleon mass is reliably described by the chiral perturbation theory, we also attempt an extrapolation using the formula provided by the $SU(3)$ heavy baryon chiral perturbation theory (HBChPT). From the chiral expansion of M_N [31] and the Feynman-Hellmann theorem (31), which will be discussed in Sec. VI, the quark mass dependence of $\langle N|S^{\text{lat}}|N\rangle$ up to the next-to-leading order is given by

$$\langle N|S^{\text{lat}}|N\rangle = -c_s - B \left\{ \frac{3}{2}C_{NNK} M_K + 2C_{NN\eta} M_\eta \right\}, \quad (20)$$

where the coefficients C_{NNK} and $C_{NN\eta}$ are written as

$$C_{NNK} = \frac{1}{8\pi f^2} \frac{(5D^2 - 6DF + 9F^2)}{3}, \quad (21)$$

$$C_{NN\eta} = \frac{1}{8\pi f^2} \frac{(D - 3F)^2}{6}. \quad (22)$$

The axial couplings F and D are phenomenologically well determined and we fix them as $D = 0.81$ and $F = 0.47$ [32]. For the pseudoscalar meson masses M_K and M_η , we use the Gell-Mann, Oakes, and Renner (GMOR) relations $M_K^2 = B(m_{ud} + m_s)$ and $M_\eta^2 = 2B(m_{ud} + 2m_s)/3$, which are valid at the leading order of the quark masses. We fix the low-energy constants f and B to the values obtained in our study of the pion mass and decay constant [28]. Note that the contributions of the decuplet baryons are ignored in this analysis.

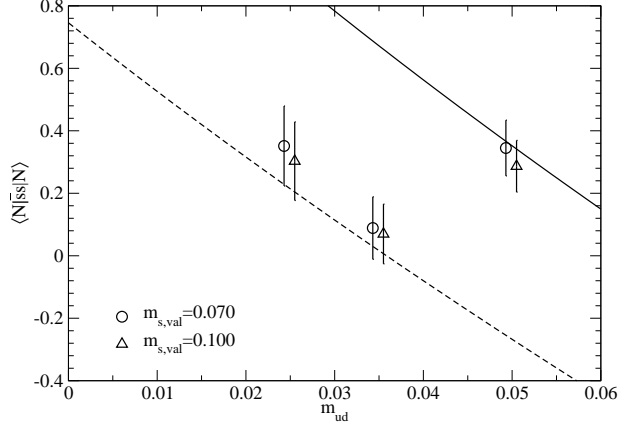


FIG. 15: The chiral fit of $\langle N|S^{\text{lat}}|N \rangle$ based on the next-to-leading order HBChPT (20). Solid and dashed lines show the fits at $m_{s,\text{val}} = 0.070$ and 0.100.

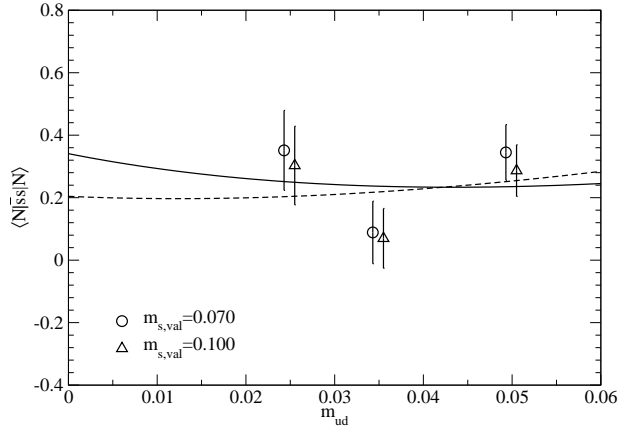


FIG. 16: The chiral fit using (23) with a higher order term.

As one can see from Fig. 15, this function does not describe the numerical data; the value of χ^2 per degree of freedom (d.o.f.) is unacceptable (~ 20). The main reason is that there is no free parameter to control the quark mass dependence, i.e., the coefficients of M_K and M_η in (20) are completely determined phenomenologically. In other words, if we leave f as a free parameter for instance, the resulting value is unreasonably large.

If we add a higher order analytic term as

$$\langle N|S^{\text{lat}}|N \rangle = -c_s - B \left\{ \frac{3}{2} C_{NNK} M_K + 2C_{NN\eta} M_\eta \right\} + c_2 M_K^2, \quad (23)$$

the fit becomes reasonable as shown in Fig. 16, for which $\chi^2/\text{d.o.f.}$ is acceptable (~ 1.9). Fit parameters obtained with (20) and (23) are summarized in Table IV. The resulting fit parameters suggest that the chiral expansion does not converge well. In fact, if we look at

	$\chi^2/\text{d.o.f.}$	d.o.f	$-c_s$	c_2	$\langle N S^{\text{lat}} N\rangle$
Equation (20)	19.5	5	5.48(6)	\dots	1.24(6)
Equation (23)	1.88	4	2.82(23)	21.2(1.8)	0.28(10)

TABLE IV: Numerical results of chiral fits using the $SU(3)$ HBChPT formulas, i.e., (20) and (23).

the individual contributions to $\langle N|S^{\text{lat}}|N\rangle$ from each term in (23), all of them are an order of magnitude larger than the data themselves, and the final result is obtained by a large cancellation.

Because of this poor convergence of the chiral expansion, we use the result of the HBChPT analysis only to estimate the systematic uncertainty. Namely, we take the result from the constant fit as a central value of $\langle N|S^{\text{lat}}|N\rangle$ at the physical quark masses. The systematic error due to the chiral extrapolation is estimated by a difference from the results of the linear (19) and HBChPT fits (23). Then, we obtain $\langle N|S^{\text{lat}}|N\rangle = 0.24(6)(16)$ at the physical quark masses. The first and second errors represent the statistical and systematic ones.

Using the experimental value of M_N , this is converted to the strange quark mass contribution to M_N defined in (1) as

$$f_{T_s} = 0.032(8)(22). \quad (24)$$

Since the combination $m_s S^{\text{lat}}$ is invariant under renormalization, no renormalization factor is required to obtain (24).

The y parameter (2) is defined as a ratio of the strange and ud quark contents. We obtain

$$y = 0.050(12)(34), \quad (25)$$

where we use an estimate $\langle N|\bar{u}u + \bar{d}d|N\rangle = 9.40(41)$ for the denominator, which is taken from our study of the nucleon sigma term [20].

A simple order counting suggests that the discretization effect is $O((a\Lambda)^2) \sim 9\%$ when we take $\Lambda \sim 500$ MeV. Other systematic errors including those of finite volume effects would not be significant, given that the statistical and systematic errors in (24) and (25) are so large ($\sim 70\%$).

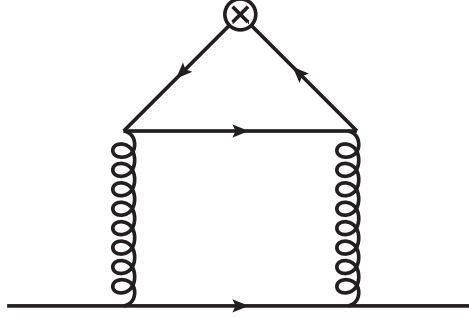


FIG. 17: The disconnected diagram contributing to the renormalization of flavor-singlet scalar operator (cross). At higher orders, the quark loop and the quark line on the bottom may be connected by an arbitrary number of gluon propagators. Since the quark-quark-gluon vertex conserves chirality, the chirality of the quark propagating in the loop does not change, as far as the regularization respects chiral symmetry.

VI. COMPARISON WITH PREVIOUS LATTICE CALCULATIONS

In this section, we emphasize an important role played by the exact chiral symmetry in the calculation of the strange quark content. Then we compare our result with the previous calculations.

A. Renormalization issue of the operator $\bar{s}s$

First, let us consider the renormalization of the $\bar{s}s$ operator in the flavor $SU(3)$ symmetric limit for simplicity. Using the flavor triplet quark field ψ , the $\bar{s}s$ operator can be written in terms of flavor-singlet and octet operators as

$$(\bar{s}s)^{\text{phys}} = \frac{1}{3} \left\{ (\bar{\psi}\psi)^{\text{phys}} - \sqrt{3} (\bar{\psi}\lambda^8\psi)^{\text{phys}} \right\}, \quad (26)$$

where λ^8 is a Gell-Mann matrix. Note that, in this section, we put the superscript “phys” on the renormalized quantities defined in the continuum theory to distinguish them from bare operators, which is in our case defined on the lattice.

In general, the singlet and octet operators may be renormalized differently

$$(\bar{\psi}\psi)^{\text{phys}} = Z_0 (\bar{\psi}\psi), \quad (27)$$

$$(\bar{\psi}\lambda^8\psi)^{\text{phys}} = Z_8 (\bar{\psi}\lambda^8\psi), \quad (28)$$

with different renormalization factors Z_0 and Z_8 . Here, we assume that the chiral symmetry is preserved in the renormalization scheme used to calculate (27) and (28). Otherwise, there is a mixing with lower dimensional operators for the flavor-singlet operator (27), as discussed below. The operator $(\bar{s}s)^{\text{phys}}$ is then expressed in terms of bare operators as

$$(\bar{s}s)^{\text{phys}} = \frac{1}{3} \{ (Z_0 + 2Z_8)(\bar{s}s) + (Z_0 - Z_8)(\bar{u}u + \bar{d}d) \}, \quad (29)$$

which implies that the $\bar{s}s$ can mix with $\bar{u}u + \bar{d}d$ unless $Z_0 = Z_8$. The difference $Z_0 - Z_8$ arises from disconnected diagrams such as those shown in Fig. 17, which exist only for the flavor-singlet operator.

When the renormalization scheme respects chiral symmetry, the disconnected diagrams vanish in the massless limit, because the quark loop starting from and ending at a scalar operator $\bar{s}s = \bar{s}_L s_R + \bar{s}_R s_L$ has to change the chirality in the loop while the change of chirality does not occur by attaching any number of gluon lines to the quark loop. It means that $Z_0 = Z_8$ is satisfied for mass independent renormalization schemes, as far as they maintain exact chiral symmetry. This also applies in the case of the overlap fermion formulation on the lattice, as there is an exact chiral symmetry guaranteed by the Ginsparg-Wilson relation [18] at finite lattice spacings [19].

Thus, the renormalization of the scalar operator reduces to a multiplicative renormalization $(\bar{s}s)^{\text{phys}}(\mu) = Z_S(\mu)S^{\text{lat}}$ with $Z_S = Z_0 = Z_8$. Here we specify the renormalization point μ for the renormalized operator $(\bar{s}s)^{\text{phys}}$. The value of $Z_S(\mu)$ is nonperturbatively calculated in [33] as $Z_S(2 \text{ GeV}) = 1.243(15)$ on our lattice. For the numerical results of f_{T_s} (24) and y (25) quoted in the previous section, the renormalization factor is unnecessary, because they are related to a renormalization invariant operator $m_s \bar{s}s$ or a ratio $\bar{s}s/(\bar{u}u + \bar{d}d)$.

As it is clear from the above discussion, the explicit violation of chiral symmetry with the conventional Wilson-type fermions induces a mixing between the strange and ud quark contents. In addition, the flavor-singlet scalar operator mixes with an identity operator, so that (29) is modified as

$$(\bar{s}s)^{\text{phys}} = \frac{1}{3} \left[(Z_0 + 2Z_8)(\bar{s}s) + (Z_0 - Z_8)(\bar{u}u + \bar{d}d) + \frac{b_0}{a^3} + \dots \right], \quad (30)$$

where the term b_0/a^3 represents the power divergent mixing contribution. This contribution from the identity operator must be subtracted as a part of the vacuum expectation value of $\bar{s}s$. Because of the cubic divergence, this results in a large cancellation toward the continuum limit.

Furthermore, since $Z_0 - Z_8$ does not vanish when chiral symmetry is violated, $\bar{s}s$ mixes with $\bar{u}u + \bar{d}d$, which induces a connected diagram contribution in the calculation of the three-point function. Since the connected diagram is larger than the disconnected contribution by an order of magnitude, the whole effect from $(Z_0 - Z_8)(\bar{u}u + \bar{d}d)$ could be substantial, even though the difference $Z_0 - Z_8$ may be small. This possibility has been neglected in most of the previous lattice calculations using the Wilson-type fermions.

B. Direct and indirect calculations

The strange quark content can also be calculated from the m_s dependence of M_N through the Feynman-Hellmann theorem

$$\langle N | \bar{s}s | N \rangle = \frac{\partial M_N}{\partial m_s}. \quad (31)$$

We refer to this method as the spectrum method in the following. Exact chiral symmetry plays a crucial role in this method, too. With the explicit chiral symmetry violation, masses of sea and valence quarks, $m_{f,\text{sea}}$ and $m_{f,\text{val}}$ (where f distinguishes the quark flavors ud and s), depend on the sea strange quark mass $m_{s,\text{sea}}$. Namely, there is an additive mass renormalization Δm

$$m_{f,\text{sea}}^{\text{phys}} = Z_m(m_{f,\text{sea}} + \Delta m), \quad (32)$$

$$m_{f,\text{val}}^{\text{phys}} = Z_m(m_{f,\text{val}} + \Delta m), \quad (33)$$

when we relate the bare quark masses on the lattice ($m_{f,\text{sea}}$ and $m_{f,\text{val}}$) to their counterparts ($m_{f,\text{sea}}^{\text{phys}}$ and $m_{f,\text{val}}^{\text{phys}}$) defined in some continuum renormalization scheme. Z_m is the multiplicative renormalization factor. With dynamical Wilson fermions, this additive mass renormalization Δm is of the cutoff order, $\sim 1/a$, and its dependence on the sea quark mass is a quantity of order unity.

Then, we can write the relevant partial derivative $\partial M_N / \partial m_{s,\text{sea}}$ calculated on the lattice in terms of the ‘‘physical’’ quark mass dependence of M_N as

$$\begin{aligned} \frac{\partial M_N}{\partial m_{s,\text{sea}}} &= \frac{\partial m_{s,\text{sea}}^{\text{phys}}}{\partial m_{s,\text{sea}}} \frac{\partial M_N}{\partial m_{s,\text{sea}}^{\text{phys}}} + \frac{\partial m_{ud,\text{sea}}^{\text{phys}}}{\partial m_{s,\text{sea}}} \frac{\partial M_N}{\partial m_{ud,\text{sea}}^{\text{phys}}} + \frac{\partial m_{ud,\text{val}}^{\text{phys}}}{\partial m_{s,\text{sea}}} \frac{\partial M_N}{\partial m_{ud,\text{val}}^{\text{phys}}} \\ &= Z_m \left[\langle N | \bar{s}s | N \rangle^{\text{phys}} + \frac{\partial \Delta m}{\partial m_{s,\text{sea}}} \langle N | \bar{u}u + \bar{d}d + \bar{s}s | N \rangle^{\text{phys}} \right], \end{aligned} \quad (34)$$

where the matrix elements appearing on the right-hand side are those with the continuum renormalization scheme. The last term must be subtracted from $(1/Z_m)\partial M_N/\partial m_{s,\text{sea}}$ to obtain the strange quark content. It requires a calculation of the light quark content $\langle N|\bar{u}u+\bar{d}d|N\rangle$, which is dominated by the connected diagram, and of the $m_{s,\text{sea}}$ dependence of Δm , which strongly depends on the details of the lattice action used in the calculation. In the literature, this subtraction was considered only in [15], where the subtraction induced a rather large statistical error.

One may avoid this problem by differentiating M_N in terms of pion and kaon mass squared, M_π^2 and M_K^2 , instead of m_s , assuming the GMOR relations $M_\pi^2 = 2Bm_{ud}$, $M_K^2 = B(m_{ud}+m_s)$. Since the quark masses appearing in the right-hand side of the GMOR relations contain the additive mass renormalization Δm , the above subtraction is not necessary. But the method introduces another uncertainty, because the GMOR relations are valid only at the leading order of the quark mass, and the higher order terms are not negligible in general. This method has been applied in the analysis of [22].

In Fig. 18 (top panel) we compare our result (25) for the y parameter plotted by a solid circle with those from previous studies using the Wilson-type actions [12–15]. Among these, [12, 13] are quenched calculations and [14, 15] contain the effects of two dynamical flavors. Rather large values $y = 0.4\text{--}0.8$ were obtained in the calculations from the nucleon three-point functions [12–14], for which the above mentioned contamination was not taken into account and large systematic error is expected. An exception is the UKQCD’s calculation with the spectrum method [15]; the subtraction of the contamination led to a large uncertainty in y .

In the same figure, we also compare our result (25) with our previous estimate $y = 0.030(16)(\pm_8^6)$ from the spectrum method [20], where the first and second errors are statistical and systematic, respectively. Because of the exact chiral symmetry satisfied in both of our calculations, these two points are free from the contamination and consistent with each other.

Recently there have been two calculations published [22, 23]. The analysis of Young and Thomas [22] fits the data from recent calculations of the baryon spectrum done by the LHPC [34] and PACS-CS [35] Collaborations, and takes a derivative in terms of M_π^2 and M_K^2 . As already mentioned, the problem of the operator mixing is avoided in this method and the authors obtained a result consistent with ours. Toussaint and Freeman [23]

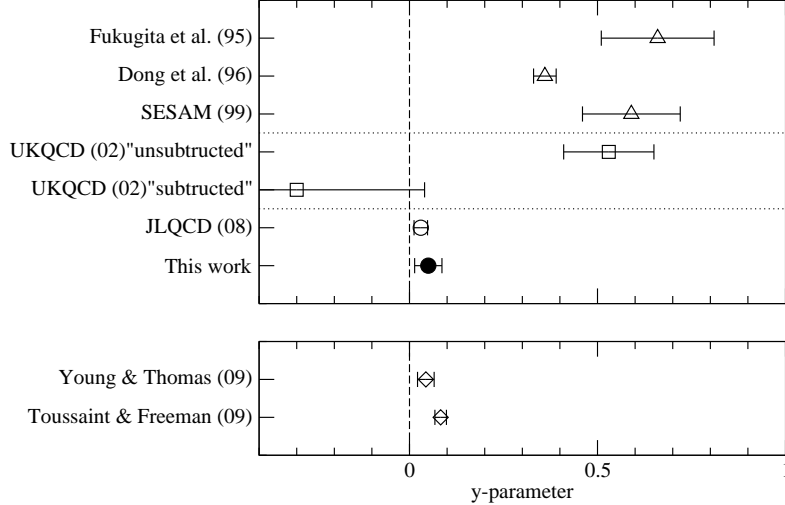


FIG. 18: (Top panel) The comparison of the y parameter with previous studies. The result in this study (25) and our estimate using the spectrum method [20] are plotted by filled and open circles. Triangles represent previous direct calculations from the nucleon three-point functions [12–14]. Squares are the results of [15] that used the spectrum method. We plot two results obtained with and without subtracting the contamination due to the chiral symmetry breaking. (Bottom panel) Two recent results [22, 23] are plotted. Values are converted to the y parameter using the quark mass ratio $m_s/m_{ud} = 27.4(4)$ [37] and the nucleon σ term [20]. The quoted errors are statistical only except for our studies and the two recent calculations [22, 23].

uses the data for the nucleon mass obtained by the MILC Collaboration using the so-called “asqtad” quark action, which is a variant of the staggered fermion formulation. They use a clever idea of extracting the derivative of the nucleon correlator in terms of the quark mass from the correlation between the nucleon correlator and the scalar density operator (the Feynman-Hellmann theorem). Since the staggered fermion has a remnant chiral symmetry, there is no problem with the operator mixing. On the other hand, there is a subtlety due to the artificial fourth root of the fermion determinant necessary for the staggered fermions, for which the Feynman-Hellmann theorem is modified. Their result appears to be slightly higher than ours.

VII. CONCLUSIONS

In this paper we calculate the nucleon strange quark content on the lattice directly from the nucleon three-point function in two-flavor QCD. Chiral symmetry is exactly preserved by employing the overlap fermion formulation on the lattice. This is crucial in the calculation of the strange quark content in order to avoid large contaminations from the operator mixing effects, that were missing in many of the previous calculations.

The lattice calculation of the disconnected diagram is technically challenging. In this work we attempted various options of the all-to-all propagator technique and the low-mode averaging together with the source and sink smearings. By optimizing those, we could finally obtain the nonzero signal at each quark mass; the value extrapolated to the physical quark masses is away from zero by 1.5 standard deviation.

The results for f_{T_s} and y are in good agreement with our previous estimate using the spectrum method [20], and favor small strange quark content $y \approx 0.05$, which is an order of magnitude smaller than previous lattice calculations without respecting chiral symmetry, which we now believe unreliable.

For more realistic calculations, we must include the dynamical strange quark in the simulation. Such a calculation is already underway using both the spectrum and direct methods [24, 36]. It is also interesting to extend this study to other baryon observables involving disconnected quark loops, such as the strange quark spin fraction of the nucleon.

Acknowledgments

Numerical simulations are performed on Hitachi SR11000 and IBM System Blue Gene Solution at the High Energy Accelerator Research Organization (KEK) under the support of its Large Scale Simulation Program (No. 09-05). This work is supported in part by the Grant-in-Aid of the Ministry of Education (No. 20105001, No. 20105002, No. 20105003, No. 20105005, No. 20340047, and No. 21684013).

[1] K. Griest, Phys. Rev. D **38**, 2357 (1988) [Erratum-ibid. D **39**, 3802 (1989)] [Phys. Rev. D **39**, 3802 (1989)].

- [2] M. Drees and M.M. Nojiri, Phys. Rev. D **48**, 3483 (1993) [arXiv:hep-ph/9307208].
- [3] A. Bottino, F. Donato, N. Fornengo and S. Scopel, Astropart. Phys. **18**, 205 (2002) [arXiv:hep-ph/0111229].
- [4] E. A. Baltz, M. Battaglia, M. E. Peskin and T. Wizansky, Phys. Rev. D **74**, 103521 (2006) [arXiv:hep-ph/0602187].
- [5] J. R. Ellis, K. A. Olive and C. Savage, Phys. Rev. D **77**, 065026 (2008) [arXiv:0801.3656 [hep-ph]].
- [6] J. Angle *et al.* [XENON Collaboration], Phys. Rev. Lett. **100**, 021303 (2008) [arXiv:0706.0039 [astro-ph]].
- [7] Z. Ahmed *et al.* [The CDMS-II Collaboration], Science **327**, 1619 (2010) [arXiv:0912.3592 [astro-ph.CO]].
- [8] T. A. DeGrand and S. Schaefer, Comput. Phys. Commun. **159**, 185 (2004) [arXiv:hep-lat/0401011].
- [9] L. Giusti, P. Hernandez, M. Laine, P. Weisz and H. Wittig, JHEP **0404**, 013 (2004) [arXiv:hep-lat/0402002].
- [10] J. Foley, K. Jimmy Juge, A. O’Cais, M. Peardon, S. M. Ryan and J. I. Skullerud, Comput. Phys. Commun. **172**, 145 (2005) [arXiv:hep-lat/0505023].
- [11] G.S. Bali, H. Neff, T. Dussel, T. Lippert, and K. Schilling [SESAM Collaboration], Phys. Rev. D **71**, 114513 (2005) [arXiv:hep-lat/0505012].
- [12] M. Fukugita, Y. Kuramashi, M. Okawa and A. Ukawa, Phys. Rev. D **51**, 5319 (1995) [arXiv:hep-lat/9408002].
- [13] S. J. Dong, J. F. Lagae and K. F. Liu, Phys. Rev. D **54**, 5496 (1996) [arXiv:hep-ph/9602259].
- [14] S. Gusken *et al.* [TXL Collaboration], Phys. Rev. D **59**, 054504 (1999) [arXiv:hep-lat/9809066].
- [15] C. Michael, C. McNeile and D. Hepburn [UKQCD Collaboration], Nucl. Phys. Proc. Suppl. **106**, 293 (2002) [arXiv:hep-lat/0109028].
- [16] H. Neuberger, Phys. Lett. B **417**, 141 (1998) [arXiv:hep-lat/9707022].
- [17] H. Neuberger, Phys. Lett. B **427**, 353 (1998) [arXiv:hep-lat/9801031].
- [18] P. H. Ginsparg and K. G. Wilson, Phys. Rev. D **25**, 2649 (1982).
- [19] M. Luscher, Phys. Lett. B **428**, 342 (1998) [arXiv:hep-lat/9802011].
- [20] H. Ohki *et al.*, Phys. Rev. D **78**, 054502 (2008) [arXiv:0806.4744 [hep-lat]].
- [21] S. Aoki *et al.* [JLQCD Collaboration], Phys. Rev. D **78**, 014508 (2008) [arXiv:0803.3197 [hep-

- lat]].
- [22] R. D. Young and A. W. Thomas, Phys. Rev. D **81**, 014503 (2010) [arXiv:0901.3310 [hep-lat]].
 - [23] D. Toussaint and W. Freeman [MILC Collaboration], Phys. Rev. Lett. **103**, 122002 (2009) [arXiv:0905.2432 [hep-lat]].
 - [24] K. Takeda, S. Aoki, S. Hashimoto, T. Kaneko, T. Onogi and N. Yamada [JLQCD collaboration], arXiv:0910.5036 [hep-lat].
 - [25] H. Fukaya, S. Hashimoto, K. I. Ishikawa, T. Kaneko, H. Matsufuru, T. Onogi and N. Yamada, Phys. Rev. D **74**, 094505 (2006) [arXiv:hep-lat/0607020].
 - [26] S. Aoki, H. Fukaya, S. Hashimoto and T. Onogi, Phys. Rev. D **76**, 054508 (2007) [arXiv:0707.0396 [hep-lat]].
 - [27] S. Aoki *et al.* [JLQCD Collaboration], Phys. Rev. D **77**, 094503 (2008) [arXiv:0801.4186 [hep-lat]].
 - [28] J. Noaki *et al.* [JLQCD and TWQCD Collaborations], Phys. Rev. Lett. **101**, 202004 (2008) [arXiv:0806.0894 [hep-lat]].
 - [29] S. Aoki *et al.* [JLQCD Collaboration and TWQCD Collaboration], Phys. Rev. D **80**, 034508 (2009) [arXiv:0905.2465 [hep-lat]].
 - [30] J. Noaki *et al.* (JLQCD collaboration), (unpublished).
 - [31] A. Walker-Loud, Nucl. Phys. A **747**, 476 (2005) [arXiv:hep-lat/0405007].
 - [32] E. E. Jenkins and A. V. Manohar, Phys. Lett. B **259**, 353 (1991).
 - [33] J. Noaki *et al.*, Phys. Rev. D **81**, 034502 (2010) [arXiv:0907.2751 [hep-lat]].
 - [34] A. Walker-Loud *et al.*, Phys. Rev. D **79**, 054502 (2009) [arXiv:0806.4549 [hep-lat]].
 - [35] S. Aoki *et al.* [PACS-CS Collaboration], Phys. Rev. D **79**, 034503 (2009) [arXiv:0807.1661 [hep-lat]].
 - [36] H. Ohki *et al.*, Proc. Sci. LAT2009 (2009) 124 [arXiv:0910.3271 [hep-lat]].
 - [37] C. Aubin *et al.* [MILC Collaboration], Phys. Rev. D **70**, 114501 (2004) [arXiv:hep-lat/0407028].